Canadian Journal of Chemistry
Revue canadienne de chimie

Magnetic alginate beads with high basic dye removal potential and excellent regeneration ability

SCHOLARONE™
Manuscripts

Magnetic alginate beads with high basic dye removal potential and excellent regeneration ability

K.Z. Elwakeel[a,b], A.A. El-Bindary[c]*, A.Z. El-Sonbati[c], A.R. Hawas[c]

[a] Chemistry Department, Faculty of science, University of Jeddah, Jeddah, Saudi Arabia

[b] Environmental Science Department, Faculty of Science, Port-Said University, Port-Said, Egypt

[c] Chemistry Department, faculty of Science, Damietta University, Damietta 34517, Egypt

*Corresponding author: E-mail address: abindary@yahoo.com (A.A. El-Bindary).

Abstract

The adsorption of crystal violet dye (CV) onto magnetic alginate composite (MAlg) from aqueous solutions was studied. Experiments were carried out as function of contact time, dosage, temperature, pH and CV concentration in the solutions. Optimum CV uptake was observed at equilibrium pH 7 and most of the CV was sorbed within 30 min. The equilibrium adsorption data were analyzed using two common adsorption models: Langmuir and Freundlich. The results revealed that Langmuir isotherm fit the experimental results well. The maximum adsorption capacity obtained from Langmuir isotherm equation was 0.113 mmol g^{-1} at 298 ± 1 K. The kinetics adsorption of CV onto MAlg composite was investigated using the pseudo first order and pseudo second order kinetic models. The results showed that the adsorption of CV onto MAlg composite followed pseudo second order kinetic model. Thermodynamic data indicated that adsorption process is endothermic and spontaneous reaction. Due to their outstanding adsorption capacities, MAlg composite is an excellent adsorbent for the removal of CV. The Composite regeneration was greater than 98.6% with 0.01 M HCl, and MAlg composite could be repeatedly utilized for CV removal with negligible loss in sorption capacity.

**Keywords:** Alginate; Adsorption; Kinetics; Thermodynamics; Regeneration

1. Introduction

Synthetic dyes are extensively used in paper, textile, food, and pharmaceutical industries. About 40,000‑50,000 tons of dyes are continuously entering the water systems due to improper processing and dying methods from these industries [1]. Many of the dyes are extremely toxic. Among various dyes, Crystal violet (CV), a synthetic basic cationic dye imparts violet color in aqueous solution. The cationic dyes are more toxic than the anionic dyes [2] as these can easily interact with negatively charged cells membrane surfaces, and can enter into cells and concentrate in cytoplasm [3]. CV is a typical triphenylmethane dye, which is widely used in textile dyeing industries, as a biological stain, dermatological agent, veterinary medicine, additive to poultry feed to inhibit propagation of harmful bacteria [4]. CV is toxic to mammalian cells and also a mutagen, mitotic poison [5] and a proven potent carcinogen [6]. It is responsible for moderate eye irritation, causing painful sensitization to light. It can cause permanent injury to the cornea and conjunctiva [7]. Inhalation of CV may cause irritation to the respiratory tracks, vomiting, diarrhea, pain, headache, and dizziness. Long term exposure may cause damage to the mucous membrane and gastrointestinal tract [8]. It is also extensively used in textile dying and paper printing. It is a mutagen and mitotic poison. Various treatment technologies like adsorption [9–13], photo degradation [14–18], coagulation flocculation [19], chemical oxidation [20,21], electrochemical oxidation [22], biological process [23] etc. are available for the removal of dye from the wastewater. Among these approaches, adsorption is regarded as an easy, economic and desirable process due to its high efficiency and ability to separate wide range of pollutants from industrial effluents [24] Alginate is one of the most extensively investigated biopolymers for removal of pollutants from aqueous solution as it is inexpensive, non-toxic and efficient. It is a natural poly saccharide extracted from brown sea weeds. Alginate is a very efficient sorbent for metal ions, However, the main drawback of its use as adsorbent is the weak mechanical strength and subsequently its weak ability for repeated use [25]. To solve this problem researcher incorporated sodium alginate in nanocomposite hydrogels [26]. The encapsulation of magnetite particles onto alginate beads is a promising solution to overcome this problem. The incorporation of magnetite within an alginate matrix improves its mechanical strength and regeneration ability. Moreover, magnetic nanoparticles can be present as a stable suspension that will not aggregate, thereby allowing uniform distribution in a reaction mixture. Within this framework, the present work focuses on the development of adsorbent combining magnetite within an alginate matrix and investigation of its performance in the removal of

crystal violet dye from aqueous solution. Here the equilibrium and kinetic behavior of CV adsorption were investigated onto magnetic alginate composite. Effects of different parameters such as pH, dye concentration, contact time, temperature, adsorbent dose on both equilibrium and the rate of adsorption were studied. Isotherms were fitted to the Langmuir, Freundlich, Dubinin-Radushkevich and Temkin models to qualify and quantify sorption sites and evaluate the mobilisation process. The batch contact time method was used to measure the adsorption rate. Kinetic parameters were then evaluated. The adsorbent was tested for its possible ability towards repeated use. The results obtained here will be useful in further applications of MAlg composite in color removal from wastewater.

2. Materials and methods

2.1. Chemicals and reagents

All materials were commercial reagent grade and used as received without further purification. The reagents used for the preparation of MAlg were $FeSO_4.2H_2O$ (Aldrich), $FeCl_3.6H_2O$ (Aldrich), ammonium hydroxide (25% Merck), sodium alginate (Aldrich, with molecular weight of 12,000–40,000) and calcium chloride (Prolabo). Demineralized water was used in all experiments. Crystal violet dye (CV) was purchased from Sigma–Aldrich chemical Co. (Scheme 1). CV stock solution of 500 mg L^{-1} for desired concentration was prepared.
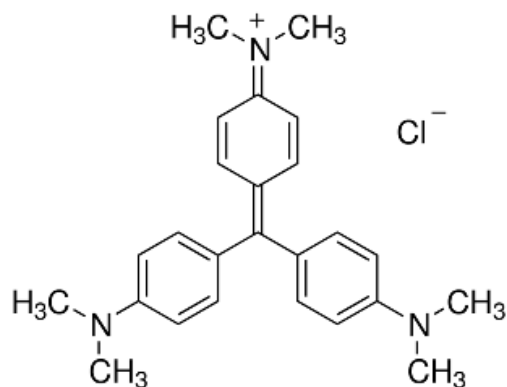
Scheme 1: Chemical structure of crystal violet dye.

2.2. Synthesis of magnetic alginate composite

3

The MAlg composite was synthesized using in situ precipitation of $FeSO_4$ and $FeCl_3$ in alkaline solution in the presence of sodium alginate. Initially, in a beaker, 30 mL of ammonium hydroxide solution was mixed with 20 mL of demineralized water to obtain an alkaline solution (7.94 mol NH_3 L^{-1}). In another beaker, 9.36 g $FeCl_3$ and 3.44 g $FeSO_4$ were dissolved in 100 mL demineralized water and then mixed with 40 mL of sodium alginate aqueous solution (2%, w/w) at 298 K for 60 min under magnetic stirring. The resultant mixture was slowly dropped into the alkaline solution at 333 K under N_2 atmosphere and vigorous mechanical stirring. The resulting black precipitate was left to react for 70 min. Then, the obtained precipitate was separated in a magnetic field and washed for three times with demineralized water to remove impurities and excess of sodium alginate not bound to Fe_3O_4 particles. It should be noted that coating of particles may occurs by electrostatic attraction between carboxylate groups of sodium Alginate, Fe^{2+} and Fe^{3+} ions of Fe_3O_4 particles. Magnetic calcium alginate beads were prepared by stirring the obtained black precipitate in 2% CaCl solution for 24 h at 303 K. The sorbent thus obtained was washed well with distilled water to remove the excess $CaCl_2$. Finally, MAlg particles were dried at 353 K under vacuum condition for 24 h to obtain final product.

2.3. Characterization of MAlg

The structure of the synthesized MAlg was examined by X-ray diffraction measurement (XRD) is recorded on X-ray diffract meter in the range of diffraction angle $2\theta=5$-80°. This analysis is carried out using $CuK\alpha1$ radiation ($\lambda=1.540598$ Å). The applied voltage and the tube current are 40 KV and 30 mA, respectively. The diffraction peaks are indexed and the lattice parameters are determined with the aid of CRYSFIRE computer program [27]. In order to confirm the structure of magnetic alginate composite were examined in dried KBr powder by recording the infrared spectra over the range of 4000–400 cm^{-1} using a Fourier transform infrared (FTIR) spectrophotometer (Jasco FTIR-4100 spectrophotometer). Thermal analysis of the risen are carried out using a Shimadzu thermo gravimetric analyzer under nitrogen atmosphere with heating rates of 10-15 °C/min over a temperature range from room temperature up to 1073 K. Scanning Electron Microscope (SEM) are carried out using JEOL JSM 6510 lv.

2.4. Sorption experiments

A stock solution (1×10^{-3} M) of CV dye was prepared in distilled water. The other solutions were obtained by dilution of the stock solution with distilled water just prior experiments. For the study of pH effect 25 mL of 2×10^{-4} M solution at different pH values (in the range 1-9) were mixed with 50 mg of sorbent (dried weight) for 2 h, and the stirring speed was maintained at 150 rpm using a reciprocal agitator, Rota bit, J.P. Selecta (Spain). The pH values were adjusted by addition of 0.1, 0.01 N HCl and 0.1, 0.01 N NaOH solutions and measured by using a pH meter (Aqualytic AL15). Samples were collected and filtrated through magnetic separation and the filtrate was analyzed for residual CV concentration using Perkin-Elmer AA800 spectrophotometer (Model AAS) at wavelength of 590 nm. The pH was not controlled during the sorption but the final pH was systematically recorded.

For sorption isotherms 50 mg of sorbent (m) were mixed with 25 mL (V) of CV solutions at different initial concentrations (C_0, ranging between 8×10^{-5} and 8×10^{-4} M) for 2 h. The pH of the solutions was initially set at 7. After solid/liquid separation, the residual concentration (C_e, mmol CV L^{-1}) was determined by a UV–vis spectrophotometer and the sorption capacity (q_e, mmol.g^{-1}) was determined by the mass balance equation:

$$q_{eq} = \frac{(C_0 - C_e)V}{m} \tag{1}$$

Where C_0 and C_e is the initial and equilibrium concentration of metal ion in solution (M), respectively, V is the volume of solution (L) and m the mass of sorbent (g).

For uptake kinetics 300 mg of sorbent were mixed with 150 mL of CV solutions (C_0: 2×10^{-4} M) at pH 7. Samples (1 mL) were collected (the sorbent being magnetically separated) at fixed times and the residual concentrations were determined by UV–VIS spectrophotometer. The agitation speed was set at 150 rpm while the temperature was maintained at 298 ± 1 K. The sorbed amount of CV per unit weight of the sorbent at time t ($q(t)$, mmol CV g^{-1}), was calculated from the mass balance equation (taking into account the decrement in the volume of the solution) according:

$$q(t) = \sum_{i=1}^{n} \frac{(C(t)_{(i-1)} - C(t)_{(i)}) \times V(t)_{(i-1)}}{m} \tag{2}$$

where $C(t)_{(i)}$ (M) is the CV concentration of the withdrawn sample number i at time t and $C(t)_{(0)} = C_0$, $V(t)_{(i)}$ (mL) is the volume of the solution in the flask at sample number i and

time t, and m is the mass of the sorbent in the flask. Here $V(t)_{(i)}$-$V(t)_{(i-1)}$ equals 1 mL (the sample volume).

The effect of temperature on the adsorption of CV was carried out in the 25 mL of dye solutions ($2x10^{-4}$ M, pH 7) with 50 mg of adsorbent for 30 min at various temperatures (293, 298, 303, 308, 313 and 318 K).

The effect of sorbent dose on CV dye removal was carried out in the 25 mL of dye solutions ($2x10^{-4}$ M, pH 7) with 0.01, 0.02, 0.03, 0.04, 0.05, 0.06, 0.07, 0.08, 0.09 and 0.1 g of adsorbent at 298 ± 1 K for 30 min.

Regeneration experiments were performed by contact of 50 mg of the sorbent with 25 mL of $2x10^{-4}$ M CV at pH 7 for 30 min. The amount of dye sorbed (and the sorption capacity) was determined by the mass balance (Eq. 1). The solution was magnetically decanted and the adsorbent was washed by distilled water. The loaded sorbent was mixed with 25 mL of 0.01 M HCl for 30 min. The regenerated sorbent was magnetically decanted, then carefully washed by alkaline solution (0.001 M NaOH) and distilled water for reuse in the second run. The regeneration efficiency (RE, %) was calculated according to the following equation:

$$RE\% = \frac{\text{Amount of adsorbed CV (mmol) at run } (n+1)}{\text{Amount of adsorbed CV (mmol) at run } (n)} \times 100 \tag{3}$$

3. Results and discussion

3.1. Characterizations of synthesized MGMA

3.1.1. Infrared spectrometry

The FT-IR spectrum of MAlg composite is presented in Figure SM1 (see Supplementary Material Section). Two absorption bands at 584 and 455 cm^{-1} corresponding to the Fe−O bands in tetrahedral and octahedral sites, confirm the spinel type structure of MAlg particles [28]. Also, the broad band's appearing in the range of 3000–3500 cm^{-1} can be attributed to stretching vibrations of O−H bonds of alginate. The asymmetric and symmetric aliphatic C−H stretching bands were observed at 2900 and 2840 cm^{-1}, respectively. The bands at 1600 and 1402 cm^{-1} were attributed to the asymmetric and symmetric stretching vibrations of carboxylate groups of alginate, respectively. The bands at 1089 and 1031cm^{-1} were attributed to the C−O stretching vibration of pyranosyl ring and the C−O stretching with contributions

6

from C–C–H and C–O–H deformations [29]. However, all of the absorption peaks confirm the coating of alginate onto the surface of magnetite (Fe_3O_4).

3.1.3. XRD analysis

The XRD pattern of the Fe_3O_4 is shown in Figure 1. The XRD spectra showed six diffraction peaks of (220), (311), (400), (422), (511), and (440), which confirm the formation of Alg–Fe_3O_4. These data revealed that the magnetite have inverse type spinel structure [30]. The XRD patterns of Alg–Fe_3O_4 show an amorphous feature by the presence of low intensity broad peak at 2θ range of 10–20 ^{o}, which can be attributed to the amorphous shell of alginate on the surface of Alg–Fe_3O_4 [31,32]. The averaged crystal size was estimated through full width at half maximum (FWHM) of the strongest reflection of the XRD pattern, using the Scherrer (Eq.1) [33]:

$$Dc = \frac{K\lambda}{\beta \cos \theta} \tag{4}$$

where k is the shape function (a value of 0.89 is used), λ is the X-ray wave length of the radiation, β is the full width at half maximum (FWHM) in radians of (311) peak in the 2θ scale, and θ is the diffraction angle. According to Scherrer equation, the averaged crystal size was calculated to be about 11.1 nm.
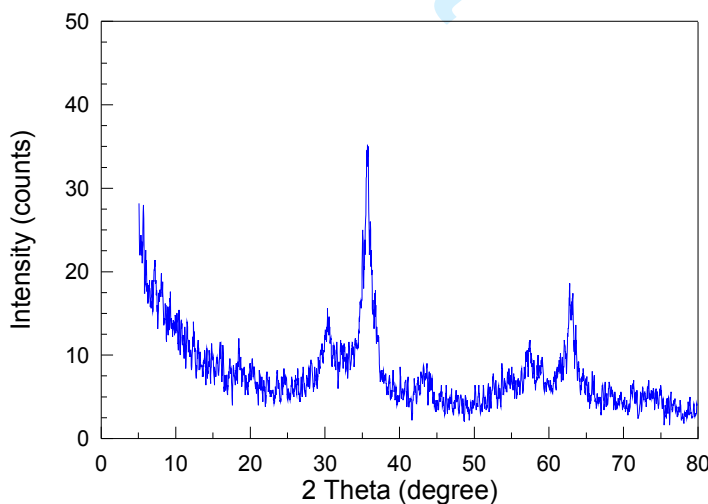
Figure 1: Powder X-ray diffraction (XRD) pattern of MAlg particles (and tentative assignment of peaks).

3.1.2. Morphology study

Scanning electron microscope is useful for determining the particle shape and appropriate size of the adsorbent. In addition, it is important tool for characterizing the surface morphology and fundamental physical properties of the adsorbent surface. Figure 2 shows the SEM analyses of the sorbent before and after CV adsorption. The SEM micrographs of the unloaded MAlg show irregular particles shape with a smooth surface, however, after CV adsorption, the surface of the adsorbent become smoother due to surface covering with dye molecules.

3.1.4. TGA analysis

TGA experiments were performed by heating Fe_3O_4 particles under nitrogen up to 1087 K in order to investigate the amount of the alginate bounded onto the surface of Fe_3O_4 particles and obtain information on their thermal stability (Figure SM2, see Supplementary Material Section). About 4.0 wt % weight loss was observed in the first stage (298–450 K) due to the loss of physically absorbed water [33]. In the second stage (450–700 K), weight loss is about 43.0 wt%, which was assigned to thermal degradation of alginate coated onto the surface of Fe_3O_4 particles. The weight loss in the third stage (700–950 K) is about 7 wt%, which may be attributed to further decomposition of alginate residues. Therefore, these results suggest the synthesized Alg–Fe_3O_4 particles are stable below 450 K. The analysis of weight loss at 950 K showed that the sorbent contains a mineral fraction close to 44 % (magnetite core material).

(a)

(b)
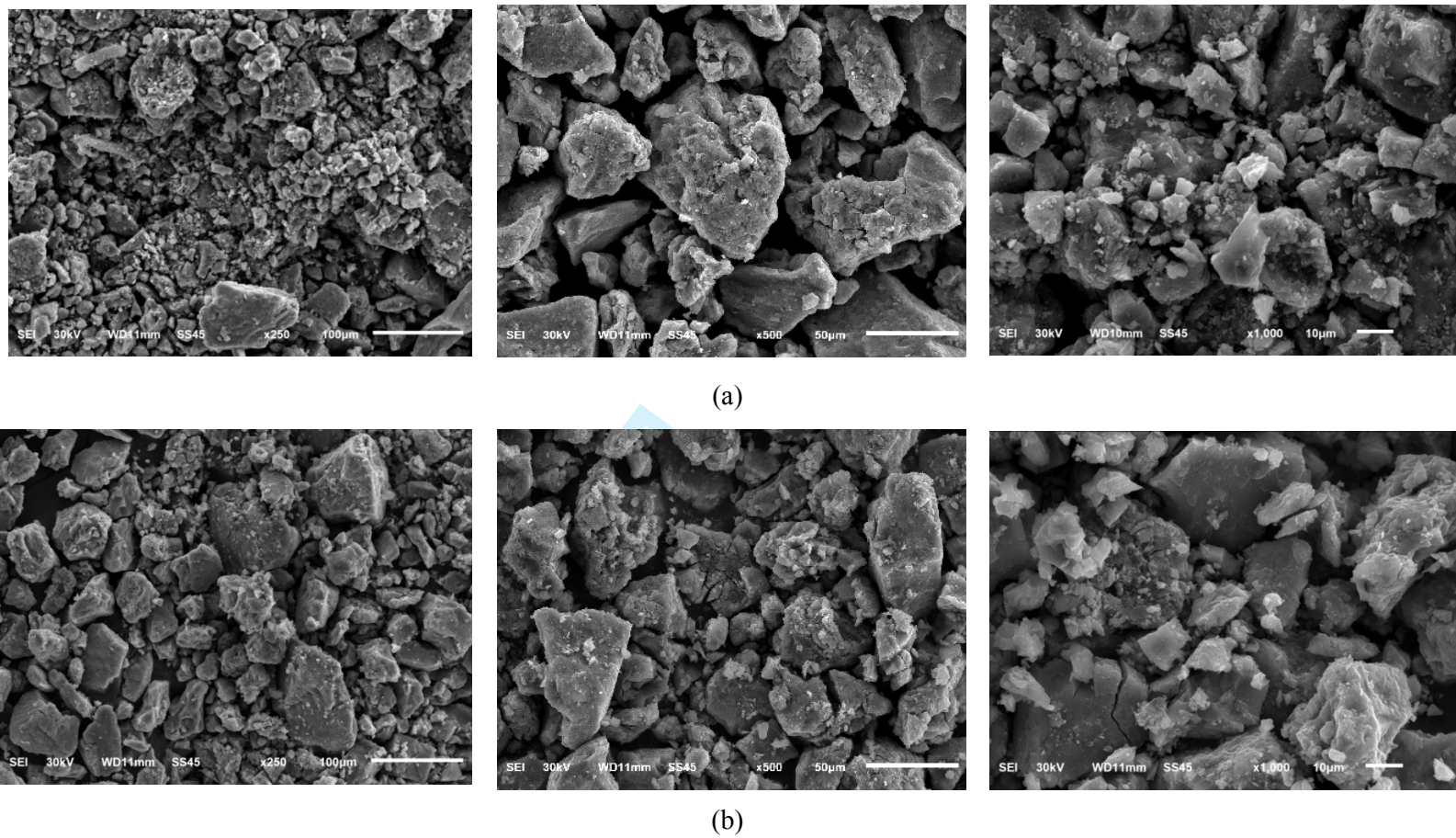
Figure 2: Scanning electron micrographs of; (a) unloaded MAlg, (b) CV loaded MAlg.

9

3.2. Adsorption analysis

3.2.1. Effect of pH on the uptake

The pH value of the dye solution is an important factor for determination of the dye adsorption [34].
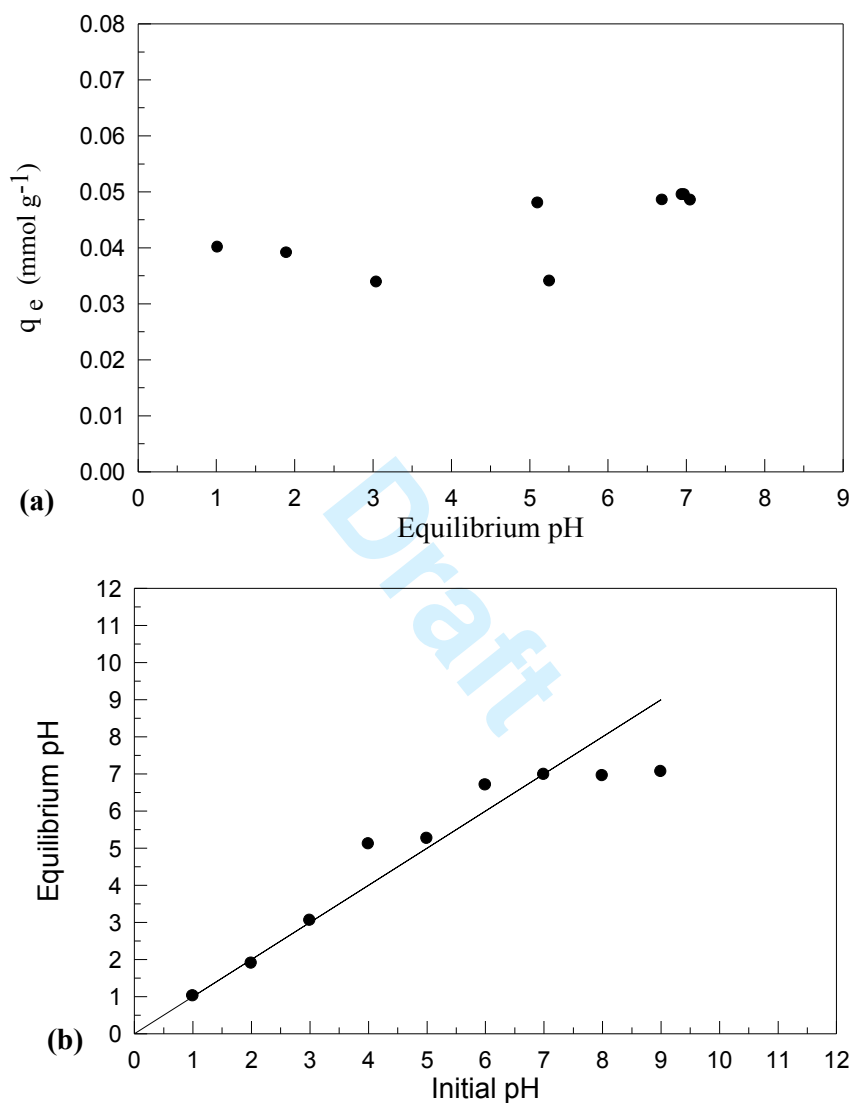
Figure 3: (a) pH effect on CV adsorption using the MAlg adsorbent: **(b)** the recorded initial

and equilibrium (final) pH: (T: 298 ± 1 K; C_0: 2x10^{-4} M).

This effect can be associated to sorbat speciation, to chemical properties of the adsorbent. The effect of the pH on the adsorption capacity of CV sorption by MAlg was studied over the initial pH (pH_i) range from (2–9). The results are shown in Figure 3a. The results suggested

that the adsorption capacity of CV on MAlg particles was pH dependent and that maximum CV removal was obtained equilibrium pH (pH$_{eq}$) 7 (Equivalent to pH$_i$ 7-9). Electrostatic interaction could play an important role on CV adsorption onto MAlg particles at various pH values. At basic medium, most of the carboxylic and hydroxyl groups in alginates are ionized and interacted with the cationic CV dye molecules via the strong electrostatic interaction, which is favorable to increase the CV absorption. Moreover, the negatively charged carboxylate groups present in alginate in basic conditions generate the electrostatic repulsion among the polymer chains. Therefore, the volume expansion in the polymer network can enhance the adsorption of cationic CV dyes due to increase in the amount of penetrating CV solution into the alginate structure [35]. In contrast, the relatively weaker CV adsorption under acidic conditions can be attributed to partial protonation of carboxylic groups (carboxylic/carboxylate ratio) of the alginate. Although the pK$_a$ value of the carboxyl groups of alginate range between 3.4 and 4.4 [36], a appreciable uptake for CV dye at acidic conditions was observed, this may be due to presence of magnetic core in the sorbent which may have additional sorption sites for CV dye. Some other researchers reported appreciable uptake for CV dye in acidic conditions [37,38].

Figure 3b shows the plot of equilibrium pH versus initial pH. For experiments performed at pH$_i$<7.0, the equilibrium pH (pH$_{eq}$) tended to increase, probably due to the sorption of protons alongside CV molecule onto the adsorbent surface. In contrast, the adsorption at higher pH (pH$_i$>7.0) caused a pH decrease: the removal of alkaline crystal violet molecule might be leads to the increase of the solution pH.

3.2.2. Adsorption kinetics

The uptake kinetics of CV using the MAlg sorbent is shown in Figure 4. The kinetic profile is characterized by two phases in the uptake: (a) a first initial step that lasts for about 10 min and counts for more than 96.5 % of total adsorption, (b) a second step that takes about 30 min and corresponds to a much slower dye accumulation. The initial section of the curve corresponds to a great availability of reactive groups (surface coverage is progressively increasing) and a large concentration gradient between the solution and both the surface and the internal sorption sites. These two conditions may explain the fast initial accumulation of CV dye. The sorption mainly occurs on the reactive alginate groups covering the surface of the sorbent. The second step, much slower, is controlled by the decrease of the concentration

Table 1: Kinetic parameters for CV adsorption

PFORE				PSORE				Weber and Morris model			Elovich equation		
k_1 (a)	$q_{e, calc}$ (b)	R^2	χ^2	k_2 (c)	$q_{e, calc}$ (b)	R^2	χ^2	Ki (d)	X	R^2	α (e)	β (f)	R^2
0.038	0.006	0.901	1.239	16.462	0.092	0.999	5.89×10^{-07}	0.00053	0.087	0.961	2.12×10^{23}	704.036	0.926

Units: (a): min^{-1}; (b): $mmol\ g^{-1}$; (c): $g\ mmol^{-1}\ min^{-1}$; (d): $mmol\ g^{-1}\ min^{0.5}$; (e): $mmol\ g^{-1}\ min^{-1}$; (f): $g\ mmol^{-1}$.
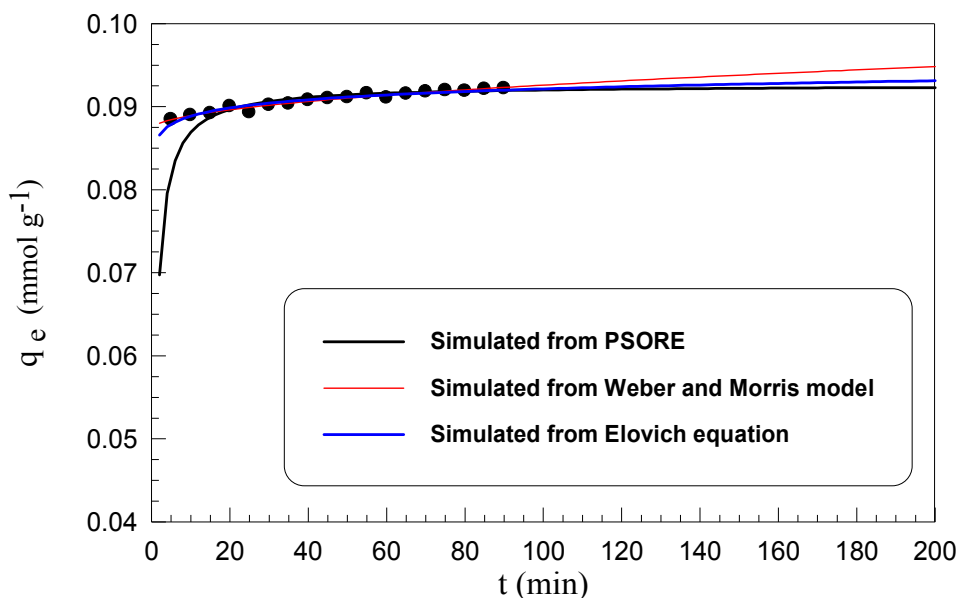
Figure 4: CV uptake kinetics using the MAlg adsorbent: (pH 7; T: 298 ± 1K; C_0: 2x10^{-4} M).

gradient and by the resistance to intraparticle diffusion and requires much longer time for reaching the equilibrium (i.e., about 90 min).

Actually the binding kinetics is controlled by a series of mechanisms including: (a) the bulk diffusion, (b) the resistance to film diffusion (or external diffusion), (c) the resistance to intraparticle diffusion, and (d) the proper reaction rate (chemical reaction rate) [39]. Usually a sufficient agitation allows neglecting the resistance to bulk diffusion and minimizes the resistance to film diffusion whose contribution in the control of uptake kinetics is mainly significant within the first minutes of contact. Experimental data have been modeled using simplified conventional equations to fit kinetic profiles and make possible the comparison of kinetic parameters for the two sorbents. Hence, the kinetics of CV sorption on the MAlg sorbent was analyzed using the pseudo-first order rate equation (PFORE) [40], the pseudo-second order rate equation (PSORE) [41], the simplified resistance to intraparticle diffusion equation [42] and the Elovich equation [43]. These models and their linear forms are reported in Table SM1 (see Supplementary Material Section), where K_1 is the pseudo-first order rate constant (min^{-1}) of adsorption and q_e and $q(t)$ (mmol dye g^{-1}) are the amounts of CV sorbed at equilibrium and time t, respectively, k_2 is the pseudo-second order rate constant (g mmol^{-1} min^{-1}), K_i is the intraparticle diffusion rate (mmol g^{-1} min$^{-0.5}$), α the initial adsorption rate

13

(mmol g^{-1} min^{-1}) and β the desorption constant (g mmol^{-1}). The validity of each model is checked by the correlation coefficient associated to the linear fits and χ^2 analysis was used to evaluate the best models to describe the metal ion sorption data. χ^2 was determined according to Eq. (5).

$$\chi^2 = \frac{(Q_{\exp} - Q_{cal})^2}{Q_{cal}} \tag{5}$$

where $Q_{\exp}$ and Q_{cal} represent the experimental Q and calculated Q from the models, respectively. The best models for describing the kinetic data can be selected if R^2 is equal to or near 1 and χ^2 is as small as possible. Table 1 reports the parameters of the different models for the studied adsorbents. Systematically, the best correlation coefficients were found for the PSORE model; this is confirmed by the plot of experimental data according the linearized forms of these models: (Figure. SM3, see Supplementary Material Section) for PFORE and PSORE, respectively, show a best fit of kinetic profiles by PSORE. In addition, the comparison of equilibrium adsorption capacities for the calculated value and the experimental value are only consistent for the PSORE model: the equilibrium sorption capacities are found close to 0.006 mmol dye g^{-1}. PSORE modeling gave value of 0.092 mmol dye g^{-1} closer from experimental value (0.086 mmol dye g) than PFORE. It was more likely to reflect that the rate-determining step might be chemical sorption and that the sorption behavior might involve an ion exchange mechanism.

However, the PSORE describes kinetics data through a global approach, and does not take into account the contribution of diffusion mechanisms in the control of the kinetics. Under these conditions, the kinetic parameters should be considered as apparent rate coefficients. The influence of resistance to intraparticle diffusion has been approached using a simplified model: the so-called Weber and Morris plot (See Table 1). The intraparticle diffusion model provides a more comprehensive approach for defining of adsorption mechanism, and the plot generally allows identifying different successive steps in the global process [42]. The Weber and Morris show linear plot (Figure SM4a, see Supplementary Material Section) does not pass through the origin suggesting that the resistance to intraparticle diffusion is not the sole rate-limiting step: other steps, e.g. resistance to film diffusion and/or reaction rate, are probably involved in the control of uptake kinetics (Figure SM4a, see Supplementary Material Section). In addition the progressive saturation of available and accessible adsorption sites influences the local equilibrium on the surface between surface sorption and

desorption. The low value of intraparticle rate constant (K_i) appearing in Table 1 indicates that the adsorbent is significantly affected by the resistance to intraparticle diffusion.

The Elovich equation was developed for modeling chemisorption processes [43]. Table SM1 (see Supplementary Material Section) displays the model equation and its linearization as well the plots to be used for determining the parameters. The values of α and β were determined from the intercept and slope, respectively, of the linear plot of q_t *vs.* ln t (Figure SM4b, see Supplementary Material Section). The values of α for the sorption of CV dye on the modified sorbents are 2.12×10^{23} (mmol g^{-1} min^{-1}). This value reflects the high affinity and fast kinetics of CV onto the MAlg sorbent, which may be attributed to the high concentration of active sites on the sorbent surface allowed for reacting with CV cations. The value of β (desorption constant) is found to be 704.03 g $mmol^{-1}$. This value is compatible with the levels cited in our previous work [44]. This is another confirmation of the high affinity of the resin for CV cations.

3.2.3. Adsorption isotherm

The adsorption isotherms reveal the specific relation between the concentration of adsorbate and the adsorption capacity of an adsorbent at a constant temperature [45]. Adsorption isotherms provide some information on how an adsorption system proceeds, and indicate how molecules of adsorbate interact with adsorbent [45].
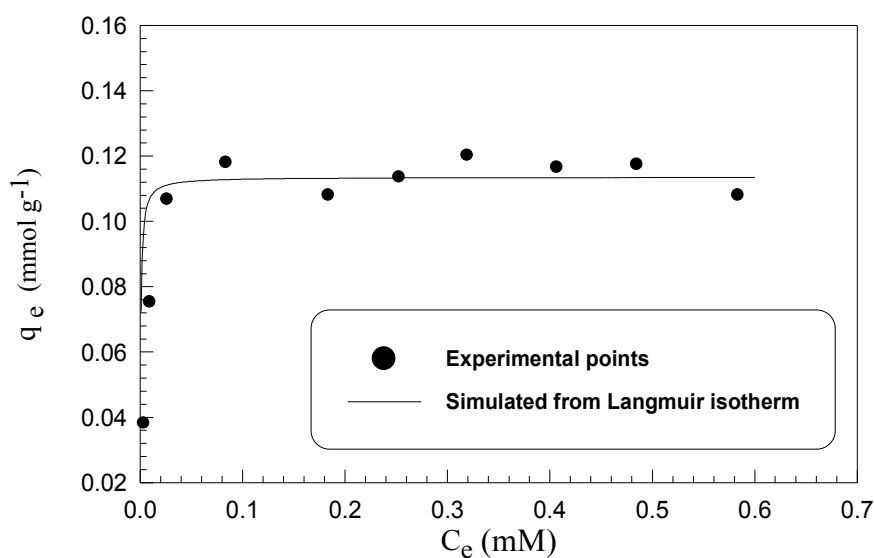
Figure 5: CV adsorption isotherms of CV dye onto the MAlg adsorbent (solid line is simulated from Langmuir equation) (pH 7; T: 298 ± 1K).

The Langmuir [46], Freundlich [47], Dubinin−Radushkevich (DR) [48], and Temkin [49] isotherm models were used to explain the sorption of CV on the MAlg sorbent. The linear and nonlinear forms of the isotherm models are shown in Table SM2 (see Supplementary Material Section), and their parameters are shown in Table 2. where q_e the adsorbed amount of dye at equilibrium concentration (mmol.g^{-1}), $q_{m,L}$ is the maximum sorption capacity (corresponding to the saturation of the monolayer, mmol.g^{-1}) and K_L is the Langmuir binding constant which is related to the energy of sorption (L mmol^{-1}), C_e is the equilibrium concentration of CV dye in solution (M). K_F (mmol.g^{-1}) (L mmol^{-1})$^{1/n}$ and n are the Freundlich constants related to the sorption capacity and intensity, respectively. K_{DR} (J^2 mol^{-2}) is a constant related to the sorption energy, q_{DR} (mmol g^{-1}) is the theoretical saturation capacity, ε (J^2 mol^{-2}) is the Polanyi potential. R (8.314 J mol^{-1}K^{-1}) is the gas constant, T is the temperature where the adsorption occurs, A_T (L mg^{-1}) is the Temkin isotherm constant, b_T (J mol^{-1}) is Temkin constant in relation to heat of adsorption.

The Langmuir isotherm models were found to be the most suitable models for describing the isotherm for the adsorption of the CV dye into the MAlg sorbent. However, the Freundlich lines deviated from the experimental data points (Figure SM5, see Supplementary Material Section). The isotherm fitting was plotted on the basis of the nonlinear equations using the model constant parameters obtained from the linear equation plot analysis. Via comparison of the R^2 values, the Langmuir isotherm resulted in very good fitting, with R^2 value of > 0.995. In addition, the Q_m calculated from the Langmuir isotherm was close to the experimental Q_{max}. The isotherm model fittings as shown in Figure 5 also show that the theoretical Langmuir lines were closer to the experimental data. Analysis of isotherm proposed by Dubinin and Radushkevich is presented in Table SM2 (see Supplementary Material Section). This isotherm was developed taking into account the effect of the porous structure of the sorbent, and the energy involved in the sorption process. The Polanyi potential (ε) given as Eq. (6) [48]:

$$\varepsilon = RT \ln\left(1 + \frac{1}{C_{eq}}\right) \tag{6}$$

R is the universal gas constant (8.314 J mol^{-1} K^{-1}) and T is the absolute temperature (K). The slope of the plot of $\ln q_{eq}$ *vs.* ε^2 (Figure SM6 see Supplementary Material Section) gives K_{DR} and the intercept yields Q_{DR} (Table SM2, see Supplementary Material Section). The D–R

16

constant (K_{DR}) can give valuable information regarding the mean energy of sorption (Ea, J mol^{-1}) by Eq. (7):

$$E_a = \frac{1}{(2K_{DR})^{0.5}} \tag{7}$$

The results of D–R isotherm are reported in Table 2. The value of the mean energy of sorption is 9.905 kJ mol^{-1}: this is consistent with the proposed mechanism of chemisorption. Indeed, it is generally admitted that 6 kJ mol^{-1} is the limit energy for distinguishing physical (below 6 kJ mol^{-1}) and chemical sorption. A comparison of the correlation coefficient values obtained from the Langmuir, Freundlich and D–R isotherm models in Table 2 reveals that the correlation coefficients for the Langmuir isotherm are somewhat higher than those for the Freundlich, D–R isotherm and Temkin models. This result suggests that the binding of dye ions may occur as a monolayer on the surface of the sorbent and that the uptake occurs on a homogenous surface by monolayer sorption. This should be confirmed by experimental observation for confirmation. The uptake can be described in terms of chemisorption as ion exchange mechanism (Protonated amino groups of DETA moiety may be exchanged with anionic dye, depending on the pH). The presence the same type of functional groups is comforting the hypothesis of homogeneous surface (or homogeneous energies of sorption). The ranking of the models as follow: Langmuir > Temkin > Dubinin and Radushkevich > Freundlich.

Table 2: Parameters of the sorption isotherm models

	Langmuir model				Freundlich model			Dubinin-Radushkevich (D-R) model					Temkin model		
$q_{m,\,exp}$ (a)	$q_{m,L}$ (a)	K_L (b)	R^2	χ^2	n	K_F (c)	R^2	Q_{DR} (a)	K_{DR} (d)	Ea (kJ mol^{-1})	R^2	χ^2	A_T (e)	b_T (f)	R^2
0.109	0.113	1756.63	0.995	0.0002	6.01	0.142	0.685	0.127	5.1×10^{-09}	9.905	0.836	0.0028	34.36	196.68	0.734

Units: (a): mmol g^{-1}; (b): L mmol^{-1}; (c): mmol g^{-1} (L mmol^{-1})$^{1/n}$; (d): J^2 mol^{-2}; (e): kJ mol^{-1}; (f): L mol^{-1}.

18

3.2.4. Influence of temperature

It is important to investigate the effect of temperature on adsorption in a view of practical application. The adsorption experiments were carried out at six different temperatures including 293, 298, 303, 308, 313 and 318 K. The adsorption capacity slightly increases from 0.0912 to 0.0997 mmol g^{-1} with the increase in the temperature from 293 to 318 K. This behavior confirms that the adsorption process of CV onto MAlg is endothermic. This observation can be attributed to increasing of the mobility of the dye molecules and rate of diffusion of adsorbate molecules across the surface of adsorbent with increasing temperature, which leads to an increase in the adsorption capacity [50]. The adsorption equilibrium constant, K_c was determined (Eq. 8) and used with the van't Hoff equation (Eq. 11) and conventional thermodynamic equation (Eq. 10) for evaluating the thermodynamic constants of the sorbents (i.e., the standard enthalpy change, ΔH^o, the standard free Gibbs energy, ΔG^o, and the standard entropy change, ΔS^o).

$$K_c = \frac{q_e}{C_e} \tag{8}$$

where q_e and C_e are equilibrium concentrations of CV on the adsorbent and in the solution, respectively.

$$\Delta G^o = -RT \ln K_c \tag{9}$$

$$\Delta G^o = \Delta H^o - T\Delta S^o \tag{10}$$

Therefore the van't Hoff equation becomes:

$$\ln K_C = \frac{-\Delta H^\circ}{RT} + \frac{\Delta S^\circ}{R} \tag{11}$$

The value of standard enthalpy change (ΔH^o) and standard entropy change (ΔS^o) for the adsorption process are thus determined from the slope and intercept of the plot of $\ln K_c$ *vs.* 1/T (Figure SM7, see Supplementary Material Section): the values of thermodynamic parameters are reported in Table 3. The positive value of ΔH^o confirms the endothermic nature of adsorption process. The negative values of ΔG^o indicate that the adsorption reaction is spontaneous. The increase in the negativity of ΔG^o with increasing temperature confirms that

the "favorability" increases with temperature. On the other hand, the positive value of the entropy change (ΔS^o) mean that the ''disorder'' of the system increases after dye adsorption.

Table 3: Standard enthalpy, entropy and free energy changes for CV adsorption

ΔH^o (kJ mol^{-1})	ΔS^o (J mol^{-1} K^{-1})	T_0 (K)	ΔG^o (kJ mol^{-1})					
			293 K	298 K	303 K	308 K	313 K	318 K
115.9	414.19	279.82	-5.45	-7.52	-9.59	-11.67	-13.74	-15.81

In industries and water purification plants the optimum temperature at which the adsorption is highly feasible and spontaneous is essential. The adsorption of dyes onto adsorbent surfaces may be either spontaneous or non-spontaneous in function of temperature. The limit temperature value corresponding to a null value of standard free energy can thus be deduced from Eq. 12. The range of temperature can be predicted from the value of temperature at which the standard free energy is zero (T_0), and then the minimal temperature for the process to being spontaneous.

$$T_0 = \frac{\Delta H^{\circ}}{\Delta S^{\circ}} \tag{12}$$

Here, the calculated value of zero standard free energy temperature (T_0) is 279.8 K. The low T_0 values indicate the feasibility of CV removal at very low temperature by the studied adsorbents.

3.2.5. Effect of adsorbent dosage

The adsorption of CV on the MAlg sorbent was studied by changing the quantity of adsorbent range of 0.01 to 0.1g of sorbent for 25 mL dye solution, with the dye concentration of 2×10^{-4} M at 298 ± 1 K and pH of 7.0. The results in Figure 6a show the CV adsorption capacity as a function of adsorbent amount. It has been found that the adsorption capacity decreases from 0.426 to 0.045 mmol g^{-1} when the dose of MAlg increases from 0.01 to 0.1 g for 25 mL dye solution. Figure 6b shows the effect of dose on the equilibrium concentration

(C/C_0) of CV by the MAlg sorbent. As the dose increases, the equilibrium concentration of CV is decreased, which is due to the increase in the adsorbent surface area of the adsorbent. The results shown indicate that the removal efficiency increases up to 99.74% (C/C_0= 0.0025) at adsorbent dose of 0.1g/25 mL. The surface of the adsorbent is composed of active sites with a spectrum of binding energies [45]. At the low dose of adsorbent, all of the sites are exposed entirely and the adsorption on the surface is saturated faster showing a higher adsorption capacity. An increase in the mass of adsorbent leads to a decrease in equilibrium adsorption capacity per unit weight of the adsorbent (q_e) because there are excess adsorbent for the limited amount of CV ions in the solution. According to the result, the adsorbent dose of 0.01 g/25 mL dye solution will achieve the maximum loading capacity for the adsorbent, and the dose of 0.1 g /25 mL will achieve the maximum removal efficiency 99.74% (C/C_0= 0.0025). So the determination of the optimum adsorbent dose depends on the design and purpose of treatment process. Thus if the water quality standard set by WHO is the target, a larger amount of adsorbent is better (0.1 g/25 mL), and if the maximum loading of the sorbent per unit mass is the target, the dose of 0.01 g/25 mL is more suitable.
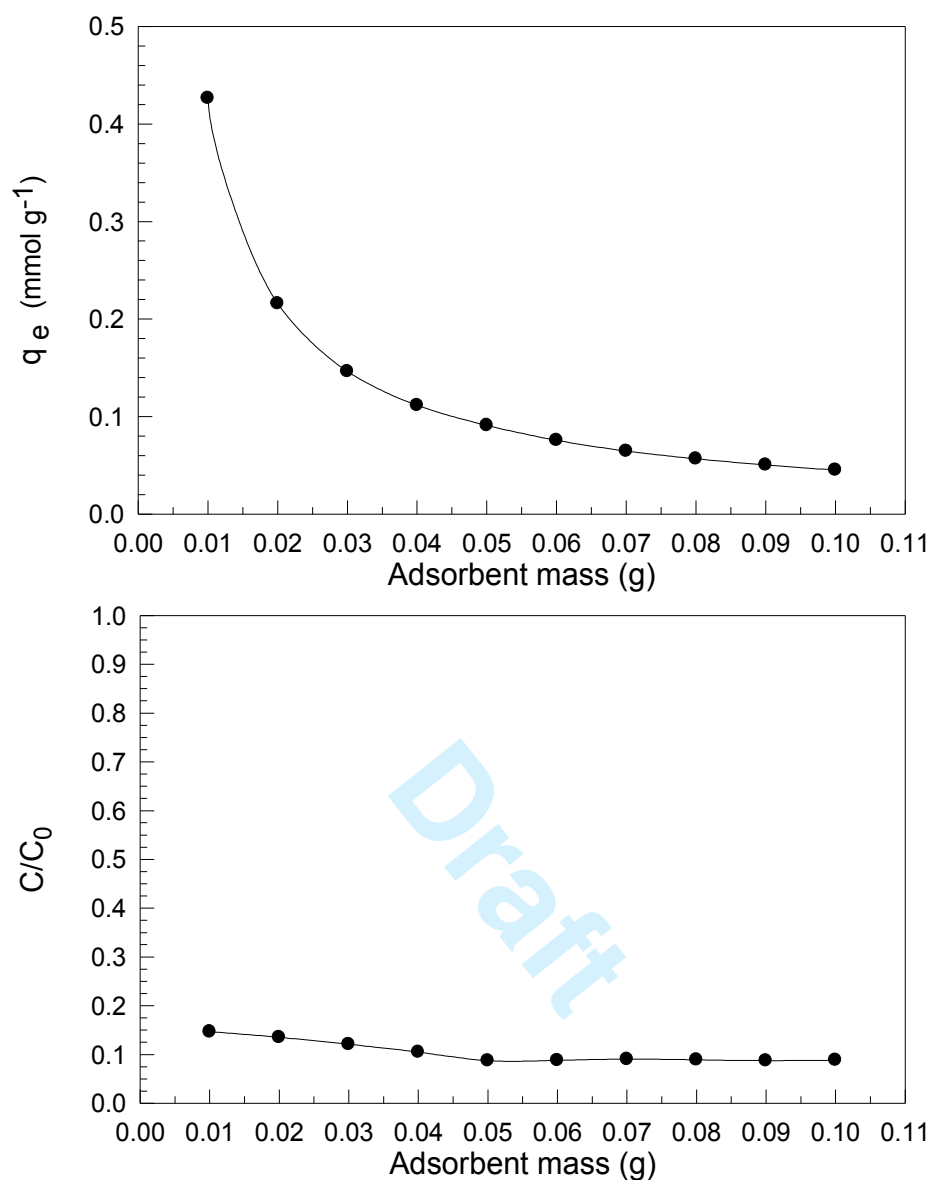
Figure 6: Effect of sorbent dose (SD) on CV adsorption using MAlg: (a) sorption capacity *vs.* SD, (b) relative residual concentration (C/C_0) *vs.* SD (C_0: 2×10^{-4} M; T: 298 ± 1K; pH 7).

3.3. Adsorbent regeneration

Regeneration of the sorbent were performed by placing 0.5 g of composite in the flask and then washed carefully by flowing alkaline solution (0.001 M NaOH) then distilled water. The composite loaded by CV was then subjected for regeneration using 0.01 M HCl. After regeneration the composite was again carefully washed with distilled water to become ready

for the second run of uptake. The regeneration efficiency for each adsorption/desorption cycle was found to be 98.6, 69.6, 94.5%. This indicates that composite has good performance for repeated use up to at least 3 cycles.

In order to identify adsorbent stability in acidic solution (Partial magnetite leaching), the concentration of Iron in the eluent solution (HCl) was analyzed by spectrophotometry (Hach DR/5000) for total iron concentration (adapted from standard Methods for the Examination of Water and Wastewater). The release of Iron from the adsorbent was negligible at pH close to 1.7; the fraction of iron leached from the sorbent did not exceed 0.2 %.

3.4. Comparison of adsorption of CV dye with various sorbents

Table 4 shows the comparison of maximum sorption capacities of the MAlg with a series of values found in the literature (together with the best operating conditions reported by respective authors). A direct comparison of sorption performance is difficult due to different experimental conditions; however, this is a useful criterion for roughly evaluating the potential of these materials. The MAlg adsorbent has a adsorption capacity of the same order of magnitude as other sorbents; although the carboxylate functionalized sugarcane bagasse with Meldrum's acid (SMA) adsorbent [51], $CaFe_2O_4$ magnetic nanoparticles [52], clay/poly(N-isopropylacrylamide) (PNIPAm) nanocomposite (CPN) hydrogels [53], core‑shell SiO_2@MgO [54], and $SnFe_2O_4$@activated carbon magnetic nanocomposite [55], showed better adsorption capacity. It is noteworthy that the MAlg sorbent has an important advantage related to their fast kinetics. The fast adsorption of CV dye reveals that MAlg adsorbent could be promising for practical application in CV dye removal from wastewater.

Table 4: Comparison of sorption capacity for CV dye with various adsorbents

Adsorbent material	Initial pH	Contact time (min)	Temperature (K)	Initial concentration (mg/L)	Sorbent dosage (g L^{-1})	Sorption capacity (mg g^{-1})	References
sugarcane bagasse modified with Meldrum's acid (SMA)	7.0	720	318	200	0.2	692.1	[51]
CaFe$_2$O$_4$ magnetic nanoparticles (MNPs)	5.5	30	298	30	0.05	10.67	[52]
clay/poly(N-isopropyl acrylamide) (PNIPAm) nanocomposite (CPN) hydrogels	3.0	720	298	10	-	1.2	[53]
SiO$_2$@MgO composite (SMC)	6.5	300	318	500	0.4	2244.85	[54]
SnFe$_2$O$_4$@activated carbon magnetic	8.0	1440	323	-	0.1	158.73	[55]
Magnetite Alginate	7	30	298	81.59	0.05	37.5	[This work]

24

4. Conclusion

Magnetite alginate as a magnetic adsorbent for the removal of crystal violet from aqueous solutions, were successfully prepared by in situ co-precipitation method and characterized via FTIR, SEM, XRD and TGA. This adsorbent exhibited high adsorption capacity towards CV. The maximum monolayer adsorption capacities are 0.092 mmol g^{-1} at pH 7 and 298 K. The nature of interaction between the dye cations and the adsorbent was found to be dependent upon the Alkalinity of the medium. The adsorption process carries out by cation exchange mechanism; however the adsorbent maintained a significant adsorption capacity at alkaline pH. The adsorption isotherms are well fitted by the Langmuir equation. Uptake kinetics is correctly fitted by the pseudo-second order rate equation. The thermodynamic parameters have been determined: the reaction is endothermic, spontaneous. The randomness of the system increases with CV adsorption. Even under drastic conditions of high ionic strength, the sorbent maintained its high sorption capacity. The adsorbents can be used successfully up to 4 times without significant loss of its original efficiency regenerated by 0.01 M HCl. This means that the studied sorbent is a promising sorbent for the efficient removal of CV dye from wastewater of textile industry.

References

[1] El-Bindary, A. A.; M. A. Diab, Hussien, M. A.; El-Sonbati, A. Z.; Eessa, A. M.
Spectrochim. Acta A **2014**, 124, 70.

[2] Boruah, P. K.; Borthakur, P. G.; Darabdhara, Kamaja, C. K.; Karbhal, I.; Shelke, M. V.;
Phukan, P.; Saikia, D.; Das, M. R. RSC Adv. **2016**, 6, 11049.

[3] Li, S. Biores. Technol. **2010**, 101, 2197.

[4] Pourjavadi, A.; Hosseini, S. H., Seidi, F.; Soleyman, R. Polym. Int. **2013**, 62, 1038.

[5] He, H.; Yang, S.; Yu, K.; Ju, Y.; Sun, C.; Wang, L. J. Hazard. Mater. 2010, 173, 393.

[6] Taher, A.; Mohsin, M.; Farooqui, M.; Farooqui, M. J. Adv. Scient. Res. **2012**, 3, 36.

[7] Sarma, G. K.; Gupta, S. S.; Bhattacharyya, K. G. J. Environ. Manage. 2016, 171, 1.

[8] Jain, S.; Jayaram, R.V. Desalination. 2010, 250, 921.

[9] Elwakeel, K. Z.; El-Bindary, A.A.; El-Sonbati, A.Z.; Hawas, A. M. RSC Adv. **2016**, 6
3350.

[10] Shojaat, R.; Saadatjoo, N.; Karimi, A.; Aber, S. J. Environ. Chem. Eng. **2016**, 4, 1722.

[11] Ali, I.; Gupta, V. K. Nat. Protoc. 2007, 1, 2661.

[12] Subbaiah, M. V.; Kim, D. S. Ecotoxicol. Environ. Saf. **2016**,128, 109.

[13] Lakshmipathy, R.; Sarada, N.C. Desalin. Water. Treat. **2016**, 57, 10632.

[14] Al-Kahtani, A. A.; Abou Taleb M. F. J. Hazard. Mater. **2016**, 309 10–19.

[15] Vaiano, V.; Iervolino, G.; Sannino, D.; Murcia, J.J.; Hidalgo, M.C.; Ciambelli, P.;
Navío, J.A. Appl. Catal. B: Environ. **2016**, 188, 134.

[16] Thangavel, S.; Thangavel, S.; Raghavan, N.; Krishnamoorthy, K.; Venugopal, G. J.
Alloys Compd. **2016**, 665, 107.

[17] Aravind, P.; Subramanyan, V.; Ferro, S.; Gopalakrishnan, R. Water Res. **2016**, 93, 230.

[18] Benjwal, P.; Kar, K. K. RSC Adv. **2015**, 5, 98166.

[19] Papic, S.; Koprivanac, N.; Bozic, A.L.; Metes, A. Dyes Pigm. **2004**, 62, 291.

[20] Bouras, H. D.; Benturki, O.; Bouras, N.; Attou, M.; Donnot, A.; Merlin, A.; Addoun, F.;
Holtz, M. D. J. Mol. Liq. **2015**, 211, 1039.

[21] Baban, A.; Yediler, A.; Lienert, D.; Kemerdere, N.; Kettrup, A. Dyes Pigm. **2003**, 58,
93.

[22] Xu, L.; Sun, Y.; Zhang, L.; Zhang, J.; Wang, F. Desalin. Water. Treat. **2016**, 57, 8815.

[23] Ledakowicz, S.; Solecka, M.; Zylla, R. J. Biotechnol. **2001**, 89, 175.

[24] Slejko; F.L. Adsorption Technology. A Step-by-step Approach to Process Evaluation
and Application, Marcel Dekker, New York, 1985.

[25] Liu, S.; Li, Y.; Li, L. Carbohyd. Polym. **2017**, 160, 62.

[26] Mahdavinia, G. R.; Aghaie, H.; Sheykhloie, H.; Vardini, M.T.; Etemadi, H. Carbohyd. Polym **2013**, 98, 358.

[27] Shirley, R. the CRYSFIRE system for automatic powder indexing:Users Manual, the lattice press, Guildford, Surrey GU 27NL, England, **2000**.

[28] Srivastava, M.; Singh, J.; Yashpal, M.; Gupta, D.K.; Mishra, R.; Tripathi, S.; Ojha, A.K Carbohyd. Polym. **2012**, 89, 821.

[29] Daemi, H.; Barikani, M.; Barmar, M. Carbohyd. Polym. **2013**, 92, 490.

[30] Xiao, Q.; Tan, X.; Ji, L.; Xue, J. Synthetic Met. **2007**, 157, 784.

[31] Fang, F. F.; Kim, J. H.; Choi, H. J. Polymer **2009**, 50, 2290.

[32] Kalyani, S.; Smitha, B.; Sridhar, S.; Krishnaiah, A. Desalination **2008**, 229, 68.

[33] Klug, H. P.; Alexander, L. E. X-ray Diffraction Procedures: For Polycrystalline and Amorphous Materials, 2nd ed., Wiley-Interscience, New York, **1974**.

[34] Inbaraj, B.S.; Chiu, C.; Ho, G. J. Yang, B. Chen, J. Hazard. Mater. **2006**, 137, 226.

[35] Wang, L.; Zhang, J.; Wang, A. Desalination **2011**, 266, 33.

[36] Goh, C. H.; Heng, P. W. S.; Chan, L. W. Carbohyd. Polymer **2012**, 88, 1.

[37] Mahdavinia, G.R.; Bazmizeynabad, F.; Seyyedi, B. Desalin. Water. Treat. **2015**, 53, 2529.

[38] Gholami, M.; Vardini, M. T.; Mahdavinia, G. R. Carbohyd. Polymer **2016**, 136, 772.

[39] Elwakeel, K. Z.; Guibal, E. Carbohyd. Polymer **2015**,134, 190.

[40] Lagergren S. Kungliga Swenska Vetenskapsakademiens Handlingar **1898**, 24, 1.

[41] Ho, Y. S.; McKay, G. Process Biochem. **1999**, 34, 451.

[42] Weber, W. J.; Morris; J. C. J. Sanit. Eng. Div. ASCE **1963**, 89, 31.

[43] Zeldowitsch; J. Acta Physicochim. URSS **1934**, 1, 364.

[44] Elwakeel, K. Z.; Alrekaby, M. M. J. Hazard. Mater. **2011**, 188, 10.

[45] Elwakeel, K. Z.; Guibal, E. Chem. Eng. J. **2015**, 281, 345.

[46] Langmuir, I. J. Am. Chem. Soc. **1918**, 40, 1361.

[47] Freundlich, H. M. F. Z. Phys. Chem. **1906**, 57A , 385.

[48] Dubinin, M. M.; Zaverina, E. D.; Radushkevich, L.V. Zh. Fiz. Khim. **1947**, 21, 1351.

[49] Temkin, M. I.; Pyzhev, V. Acta physiochim. URSS **1940**, 12, 217.

[50] Patra, A. S.; Ghorai, S.; Ghosh, S.; Mandal, B.; Pal, S. J. Hazard. Mater. **2016**, 301, 127.

[51] Ferreira, B. C. S.; Teodoro, F. S.; Mageste, A. B. Ind. Crops Prod. **2015**, 65, 521.

[52] An, S.; Liu, X.; Yang, L.; Zhang, L. Chem. Eng. Res. Design, **2015**, 94, 726–735.

[53] Zhang, Q.; Zhang, T.; He, T.; Chen, L. Appl. Clay Sci. **2014**, 90, 1.

[54] Pei, Y.; Wang, M.; Tian, D.; Xu, X.; Yuan, L. J. Colloid. Interf. Sci. **2015**, 453, 194.

[55] Rai, P.; Gautam, R. K.; Banerjee, S.; Rawat, V.; Chattoapadhyaya, M. C. J. Environ. Chem. Eng. **2015,** 3, 2281.